Vietnam Journal of Science and Technology ***60*** *(1) (2022) 49-60*

doi:10.15625/2525-2518/15778

LUMINESCENCE TEMPERATURE ANTI-QUENCHING IN CdSe/CdS CORE/SHELL AND CdSe/CdS/ZnS CORE/DOUBLE SHELL NANOSTRUCTURES

Nguyen Dieu Linh[1], Nguyen Thi Thuy Lieu[2], Nguyen Thi Minh Hien[3], Nguyen Xuan Nghia[3, *]

[1]*University of Science and Technology of Hanoi, 18 Hoang Quoc Viet, Cau Giay, Ha Noi, Viet Nam*

[2]*Posts and Telecommunications Institute of Technology, Km10 Nguyen Trai, Ha Noi, Viet Nam*

[3]*Institute of Physics, Vietnam Academy of Science and Technology, 18 Hoang Quoc Viet, Ha Noi, Viet Nam*

[*]Email: *nxnghia@iop.vast.vn*

Received: 20 December 2020; Accepted for publication: 4 November 2021

Abstract. Luminescence temperature anti-quenching (LTAQ) was investigated on CdSe/CdS core/shell and CdSe/CdS/ZnS core/double shell nanostructures prepared by hot injection method. They have the same core size, CdS shell thickness ranging from 1 to 5 monolayer (ML) and ZnS shell thickness of 2 ML. Temperature-dependent photoluminescence (PL) spectra of the purified core, core/shell, and core/double shell samples were comparatively investigated over a temperature range of 79 - 460 K. The LTAQ phenomenon was observed for the core/shell and core/double shell nanostructures and is reversible. The fluorescence recovery magnitude and the temperature range in which the LTAQ process occurs depends on the thickness and composition of the shell surrounding the core. Analysis of the temperature-dependent spectral characteristics shows an increase in compression strain in the CdSe core when increasing the shell thickness. The cause of the LTAQ phenomenon is attributed to the rearrangement of the atoms at the core/shell and shell/shell interfaces in the investigated nanostructures due to thermal expansions of the core and shell crystalline lattices. The linear dependence of integrated emission intensities of CdSe/CdS (1 ML) and CdSe/CdS (3 ML) samples on temperature in the ranges of 220 - 360 K and 270 - 340 K, respectively, opens up the prospect of creating temperature sensors for biomedical applications.

Keywords: Core/shell nanostructure, luminescence temperature anti-quenching, interface restructuring.

Classification numbers: 2.1.1, 2.4.1, 2.5.3.

1. INTRODUCTION

The primary solution to increasing the photoluminescence quantum yield (PLQY) and optical stability of nanocrystals (NCs) is to create a passive coating on the NCs' surface. This solution can remove surface defects, therefore reducing unwanted emission quenching. For

eliminating surface effect, passivation using inorganic materials with wide band gaps is a widely used solution. The PLQY of NCs are highly sensitive to minor changes in preparation parameters. This shows that the surface structure is a crucial factor in the appearance of states in the band gap, causing exciton luminescence quenching.

Luminescence temperature quenching is a common phenomenon in fluorescence materials and is attributed to the capture of carriers by temperature-induced activations of trap centers and multiphonon-assisted nonradiative electron relaxation at high temperatures [1 - 3]. However, luminescence temperature anti-quenching (LTAQ) was also observed in (i) phosphors containing intentional defects [4, 5], or doped with rare earths [6] or lanthanides [7]; (ii) quantum dots and core/shell-type nanostructures such as CdSe [8], CdSe/CdTe [9], CdSe/ZnS [10], and CdSe/CdS/CdZnS/ZnS [11] dispersed in organic mediums; and (iii) ZnS/CdS:Mn/ZnS doped quantum well-quantum dots [12]. This has created prospects for applications in contactless optical thermometry. With advantages such as size-tunable absorption and emission energies, good photostability, high PLQY and significant temperature dependence of photoluminescence (PL), core/shell-type nanostructures are of interest for applications in optical temperature probes [13].

The LTAQ phenomenon in the core/shell nanostructures is described to be caused by the restructuring of their surfaces in relation to the phase change of the surrounding organic medium [8,9]. Surface restructuring is dependent on the surface energy of NCs, and therefore is governed by the size, shape, and ionic properties of the crystal lattice, as well as the surface passivation. Although the relation between NC surface restructuring and passivation is one of the key factors influencing the optical properties of chemically prepared semiconductor NCs, the role of semiconductor NC surface and its interaction with the passive shell is not yet fully understood.

In this study, the LTAQ phenomenon is investigated for CdSe bare-cores, CdSe/CdS core/shell and CdSe/CdS/ZnS core/double shell nanostructures prepared using the hot injection method. To eliminate the influence of the ligands used during preparation, the NC samples were purified prior to the investigation of their characteristics. Temperature-dependent PL spectra of the samples are measured in the temperature range from 79 to 460 K. The nature of the LTAQ phenomenon is discussed based on the temperature-dependent spectral characteristics such as PL intensity, emission energy and temperature coefficient (in the Varshni expression).

2. MATERIALS AND METHODS

2.1. Materials

Initial chemicals including cadmium oxide (CdO, 99.99 %), selenium powder (Se, 99.999 %), oleic acid (OA, 90 %), trioctylphosphine (TOP, 97 %), and octadecene (ODE, 90 %) were purchased from Aldrich and used as received without further purifications.

2.2. Synthesis of CdSe/CdS core/shell and CdSe/CdS/ZnS core/double shell nanostructures

The CdSe bare-core NCs, as well as the CdSe/CdS core/shell and CdSe/CdS/ZnS core/double shell nanostructures were prepared by the hot injection method. The Se precursor solution was created by dissolving Se powder in TOP and ODE at 50 ^{o}C. To grow CdS and ZnS shells, the S stock solution was prepared by heating a mixture of S powder and ODE at 80 ^{o}C. The Cd and Zn precursor solutions were obtained by dissolving CdO and ZnO in OA and ODE mixtures, respectively, at 200 ^{o}C.

The CdSe bare-core NCs were synthesized with a Cd:Se ratio of 1:2 and an OA concentration in the reaction solution of 0.05 M. The Se precursor solution was quickly injected into a flask containing Cd precursor solution heated to 280 ^{o}C. Afterwards, the reaction solution temperature was rapidly reduced to 200 ^{o}C and maintained for 10 mins to grow the NCs, and the flask was then cooled down to room temperature.

The CdSe/CdS core/shell nanostructures were prepared using purified CdSe bare-core NCs. The CdS shell was formed with a Cd:S molar ratio of 1:1, a Cd concentration in ODE of 0.04 M and an OA:Cd ratio of 6:1. The solution containing CdSe bare-cores was quickly injected into a flask containing ODE heated to 190 ^{o}C. Afterwards, the Cd and S precursor solutions were slowly injected into the flask to create the CdS shell on the surfaces of CdSe bare-cores. The quantities of CdO and S powder needed for each monolayer (ML) were precalculated based on the size and concentration of the used CdSe bare-cores, as well as the lattice constant of CdSe and CdS [14]. For convenience, the calculated values are used to describe the thickness of the CdS shell in terms of number of MLs. The CdSe/CdS/ZnS core/double shell nanostructures were similarly created. Preparation of precursor solutions, bare-cores and the core/shell and core/double shell nanostructures were performed under pure nitrogen gas.

The investigated samples include CdSe bare-core NCs, CdSe/CdS core/shell nanostructures with shell thicknesses of 1-5 ML, and CdSe/CdS/ZnS core/double shell nanostructures with CdS and ZnS shell thicknesses of 3 and 2 ML, respectively. The NCs were isolated from crude solutions by mixing the solutions with isopropanol at 1:3 volume ratio and centrifuging at a speed of 14000 rpm for 5 min. The purification process was repeated three times, and then the NC samples were dispersed in toluene.

2.3. Sample characterization

Transmission electron microscopy (TEM) and high-resolution transmission electron microscopy (HRTEM) images of CdSe bare-core, CdSe/CdS core/shell and CdSe/CdS/ZnS core/double shell samples were recorded using the JEM 1010 and JEM 2100 microscopes (Jeol), respectively. Powder X-ray diffraction (XRD) measurements were conducted employing the D5005 X-ray diffractometer (Siemens) with Cu-K_{α} radiation wavelength of 0.15406 nm. Raman spectra were obtained from the LabRam HR Evolution spectrometer (Horiba) with the laser wavelength of 532 nm. The PL measurements were performed for the dried NC samples using the LabRam-1B spectrometer (Jobin-Yvon) with the excitation wavelength of 488 nm from the Ar^{+} laser. Low optical excitation power was used to prevent sample heating. Sample temperature was changed in the range of 79 - 460 K employing the Linkam-600 apparatus. Samples were adjusted to their initial position after each change of measurement temperature. The PL spectra were normalized with optical density at the excitation wavelength of 488 nm.

3. RESULTS AND DISCUSSION

3.1. Crystal structure, phonon characteristics and morphology of the samples

To confirm the formation of CdS shell around the CdSe core, the crystal structure, phonon characteristics and morphology of the samples were investigated. XRD patterns of the CdSe bare-core and CdSe/CdS core/shell NCs with the shell thicknesses of 0, 1, 3 and 5 ML are displayed in Figure 1(a). The 2θ diffraction angle positions of bulk CdSe and CdS materials having zinc blende structure (JCPDS cards No. 19-191 and No. 10-454, respectively) are shown

for comparison. The XRD pattern of the CdSe bare-core is characterized by the (111), (220), and (311) diffraction peaks centered at 25.6, 42.4, and 49.7°, respectively. The non-appearance of diffraction peaks at 2θ angles of approximately 37° and 48° on the CdSe/CdS samples' XRD patterns indicates that the CdS shells also have zinc blende structure. The increase in the CdS shell thickness from 1 to 5 ML results in the gradual shift of the (111) peak toward larger 2θ angle (from 25.6 to 26.3°) reflecting a compression strain in CdSe core and accompanied by a tensile strain in the CdS shell due to the smaller lattice constant of the CdS as compared to the CdSe [15 - 17].

Other evidence of CdS shelling on the CdSe core surface can be obtained from the samples' Raman spectra. As can be seen from Figure 1(b), beside the longitudinal optical mode of the CdSe bare-core (LO_{CdSe}) at 206 cm^{-1}, the formation of the CdS shell layer surrounding the CdSe core leads to the appearance of LO_{CdS} mode [16, 18 - 22], and it becomes stronger and narrower with the shell growth. Both modes shift progressively toward higher wavenumber (from 208 to 211 cm^{-1} for LO_{CdSe} mode and from 277 to 295 cm^{-1} for LO_{CdS} one) as the CdS shell thickness increased from 1 to 5 ML. In agreement with the XRD results, the shift of LO_{CdSe} peak to higher frequency exhibits the compression strain in the CdSe core. Meanwhile, the strong shift of LO_{CdS} peak mainly results from phonon confinement [18, 19, 21].

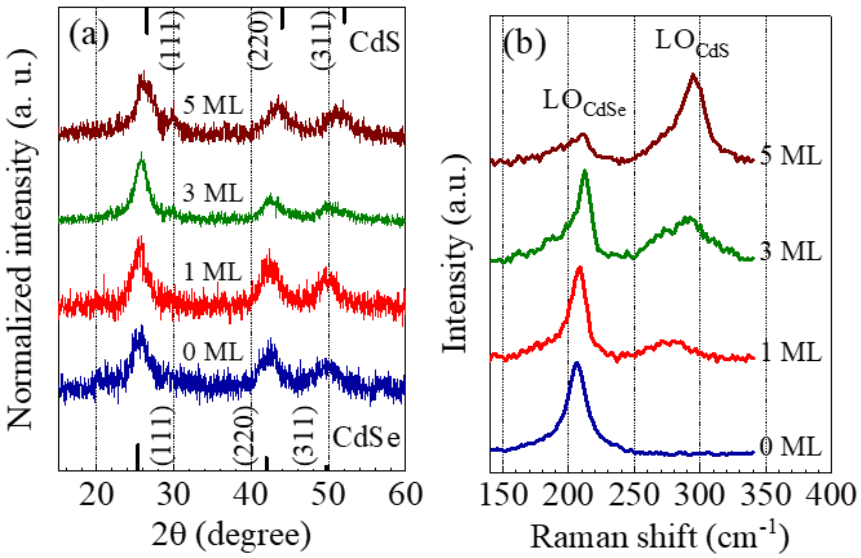

Figure 1. (a) XRD patterns and (b) Raman spectra of CdSe bare-core and CdSe/CdS NCs with different shell thicknesses.

Figures 2(a) and 2(b) are the TEM and HRTEM images of the CdSe bare-core and CdSe/CdS (3 ML) core/shell NCs, respectively. The NCs have a near-spherical shape and are relatively homogeneous. The bare-core and core/shell NCs have an average size of 4.5 and 8.4 nm, respectively. Thus, the monolayer number of the CdS shell (equals to the ratio of shell thickness to the CdS zinc blende crystal's lattice constant [23]) is 3.3 ML and approximately equals to the calculated value.

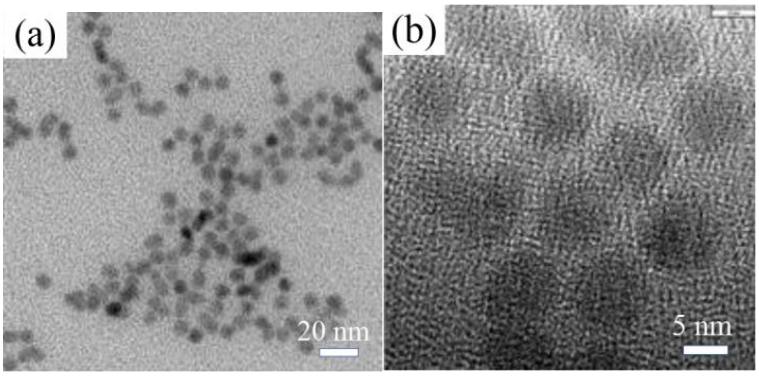

Figure 2. (a) TEM image of CdSe core NCs, and (b) HRTEM image of CdSe/CdS(3 ML) core/shell NCs.

3.2. Effect of shell thickness on the luminescence efficiency of the samples

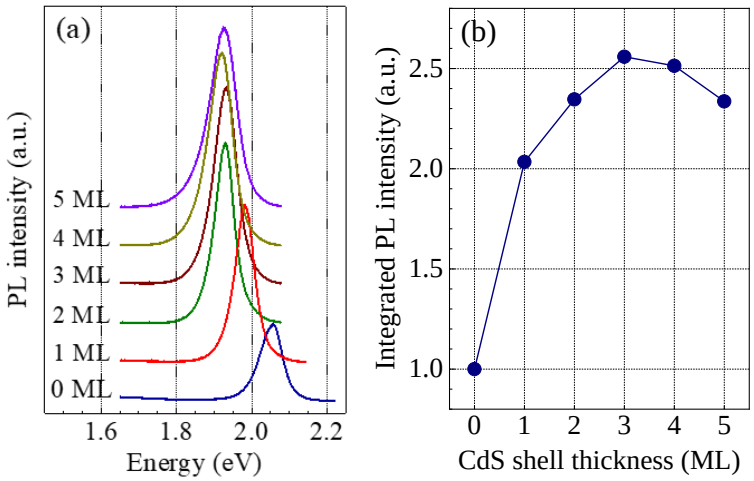

Figure 3. (a) PL spectra of CdSe/CdS samples with different CdS shell thicknesses, and (b) their integrated PL intensity as a function of shell thickness.

Figure 3(a) shows the PL spectra of the CdSe bare-core sample and the CdSe/CdS core/shell samples with shell thicknesses ranging from 1 to 5 ML. As can be seen here, the emission peak of the CdSe core is strongly shifted towards lower energy (~ 125 meV) with shell thicknesses up to 2 ML and is insignificantly shifted afterwards. This strong emission peak shift is mostly related to the narrowing of the CdSe/CdS core/shell nanostructure's optical band gap, which can be explained in two separate ways. First, due to the relatively insignificant difference in the band gap energy between CdS and CdSe, which cannot fully confine the CdSe core's electrons, they can easily move into the CdS outer shell. Meanwhile, the majority of the holes are being confined in the core due to their larger effective mass [16, 17, 19, 22, 24]. The separation of electrons and holes in the NC's different spatial domains caused a decrease in exciton confinement energy, therefore shifting the CdSe/CdS nanostructure's absorption edge towards lower energy [18, 25]. Second, for direct band gap semiconductors such as CdSe, the deformation potential of the conductive band is greater than that of the valence band (as it is inversely proportional to the state density). Therefore, the band gap energy is decreased as the core/shell nanostructure's strain increases, causing the absorption and luminescence spectra of

the CdSe/CdS nanostructure to be shifted to lower energy with increasing the shell thickness [26]. However, when the shell reaches a certain thickness, the outward movement of the electrons is limited, and the confinement energy remains unchanged [27]. This specific thickness is dependent on the height of the potential barrier between the core and shell and/or the core/shell structure's strain. In the case of the CdSe/CdS samples described above, this thickness is approximately 2 ML.

The comparison of the integrated PL intensities of CdSe/CdS samples with different shell thicknesses to that of the CdSe bare-core sample (normalized to 1) in Figure 3(b) demonstrates that the emission efficiency of CdSe/CdS NCs increases with the shell thickness, reaching its maximum of ~ 2.55 with a shell thickness of 3 ML, and then decreases as the shell thickness further increases. The obtained results are in good agreement with previously published ones [18,28], showing that the dependence of the integrated PL intensity on shell thickness described in Figure 3(b) is the nature of the samples containing these materials. The decrease in the integrated PL intensity of CdSe/CdS nanostructures is related to the strain in the CdS shell. As the CdS shell thickness increases above 3 ML, the strain caused by misfit in lattice parameter between CdSe and CdS may result in dislocations and small angle boundaries relaxing the nanocrystal structure [15, 24]. These defects may be non-radiative recombination sites within the CdS shell, capturing carriers delocalized into the shell region and causing a decrease in their integrated PL intensities [15, 16, 18, 25].

3.3. Luminescence temperature anti-quenching in core/shell and core/double shell nanostructures

In general, the increase in semiconductor's temperature usually results in the shift of the emission peak towards lower energy, the increase in full width at half maximum of the peak, and the decrease in their PL intensity. Figure 4 shows the change in PL spectra of the CdSe bare-core and CdSe/CdS core/shell samples with shell thicknesses of 2 and 4 ML at temperatures ranging from 79 to 430 K. The emission peak shifts towards lower energy and broadens as the temperature increases. However, the change in the samples' emission intensity with temperature is anomalous. When the temperature reaches a certain value, the PL intensity slightly increases instead of decreasing, and then begins to decrease at higher temperatures.

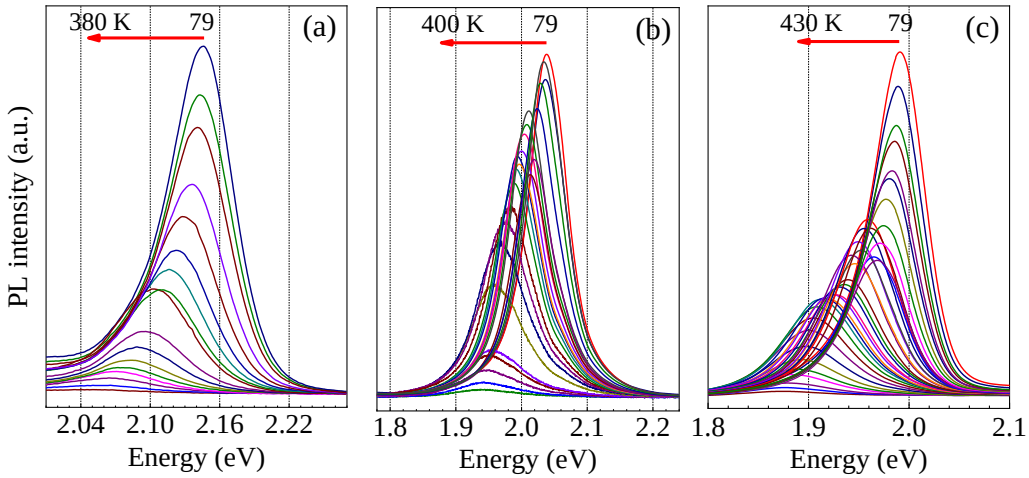

Figure 4. Temperature-dependent PL spectra of CdSe bare-core NCs (a), CdSe/CdS (2 ML) (b) and CdSe/CdS (4 ML) (c) core/shell nanostructures.

The temperature-dependent changes in emission intensities of CdSe bare-cores and CdSe/CdS NCs with different shell thicknesses are described in Figure 5(a). The emission intensities of all samples at 79 K have been normalized to one. As can be seen, luminescence recovery occurs on all samples but with different magnitudes depending on their shell thicknesses. As the shell thickness increases, the recovery magnitude increases, reaching its maximum in the investigated temperature range for the CdSe/CdS (3 ML) sample, and then decreases. Notably, there is a significant increase in the core/shell samples' emission intensity in the temperature range of 180 - 340 K.

To explain this anomalous phenomenon, the dependence of the CdSe bare-core and CdSe/CdS NC samples' PL characteristics on their temperature were investigated in detail based on the Varshni expression [29]:

$$E_g(T) = E_{g0} - \alpha \frac{T^2}{(T+\beta)}$$

where $E_g(T)$ is the band gap energy at temperature T (K), E_{g0} is the band gap energy at 0 K, α is the thermal coefficient, and β is approximately equal to the material's θ_D Debye temperature. The temperature-dependent change in emission energy of the CdSe bare-core and CdSe/CdS NCs with shell thicknesses of 2 and 4 ML is well described using the Varshni expression as shown by the solid lines in Figure 5(b). The obtained value of β (Debye temperature) from the CdSe bare-core sample is 112 K, which is relatively smaller than that of the CdSe bulk crystal (139 K) and is attributed to the "softening" of the crystal lattice as the size decreases [30]. The obtained value of α from the CdSe bare-core sample is 3.87×10^{-4} eV/K, in the determined range for CdSe bulk crystals ($(2.8 - 4.1) \times 10^{-4}$ eV/K [2]). The solid line in the inserted graph in Figure 5(b) shows the increasing tendency of α with the CdS shell thickness. Notably, the α coefficient significantly increases with shell thicknesses larger than 3 ML, reflecting a stronger change of the strain in the CdSe core.

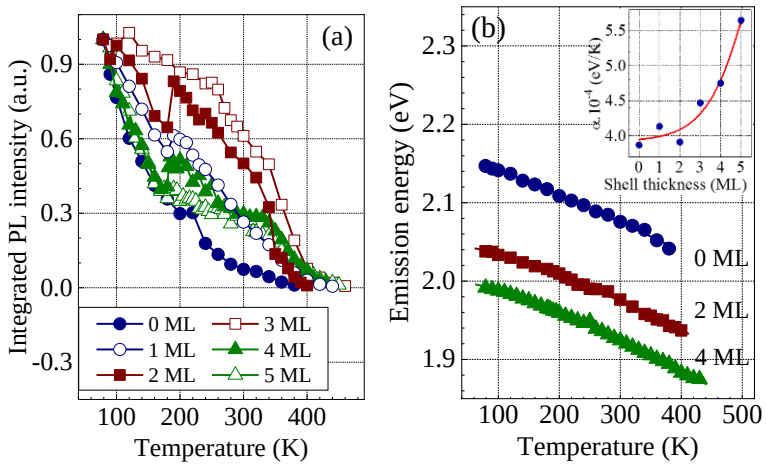

Figure 5. The dependencies of integrated PL intensities (a) and band edge emission energies (b) of CdSe core and CdSe/CdS core/shell samples on temperature. Inserted graph in Figure 5(b) exhibits change tendency of thermal coefficient α for CdS shell thickness.

To better understand the luminescence recovery mechanism, the CdSe/CdS (5 ML) sample's PL spectrum was investigated with its temperature decreasing from 300 to 79 K, then

increasing back to 300 K. The measurements were performed at the same position on the sample's surface. The results are shown in Figures 6(a) and 6(b). As can be seen from Figure 6(c), the two integrated PL intensity curves measured with increasing and decreasing temperatures almost overlap, demonstrating LTAQ's reversibility.

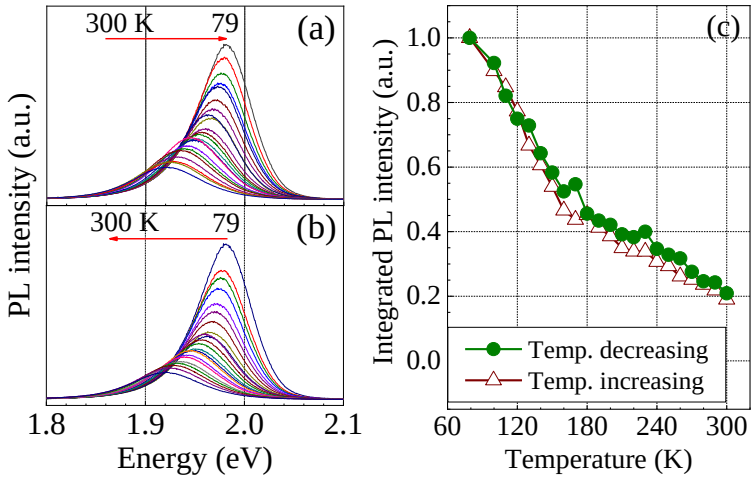

Figure 6. (a, b) PL spectra of CdSe/CdS (5 ML) measured at the same position on the sample surface, and (c) integrated emission intensities obtained when decreasing and increasing temperatures in the range of 79-300 K.

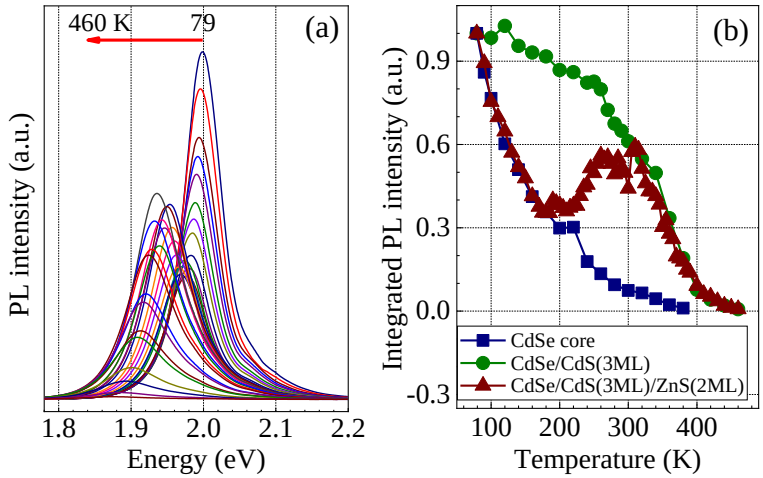

Figure 7. (a) Temperature-dependent PL spectra of the CdSe/CdS (3 ML)/ZnS (2 ML) sample; (b) Comparison of temperature-dependent integrated PL intensities of CdSe, CdSe/CdS (3 ML) and CdSe/CdS (3 ML)/ZnS (2 ML) samples.

Intense luminescence recovery was also observed in CdSe/CdS (3 ML)/ZnS (2 ML) core/double shell nanostructures as shown in Figure 7(a). The comparison between the temperature-dependent integrated emission intensities of the CdSe bare-core, CdSe/CdS (3 ML) and CdSe/CdS (3 ML)/ZnS (2 ML) samples in Figure 7(b) shows that the integrated emission intensity of the CdSe/CdS (3 ML)/ZnS (2 ML) sample coincides with that of the CdSe bare-core in the temperature range of 79-180 K, similar to CdSe bare-core passivated by CdS shells with thicknesses of 4 and 5 ML (Figure 5(a)). Further increases in sample temperature results in

luminescence recovery, reaching the maximum intensity of 0.6 times the PL intensity at 79 K, then nearly coincides with that of the CdSe/CdS (3 ML) sample in the temperature range of 320-460 K. The results in Figures 5(a) and 7(b) suggest that it is possible to change the emission intensity-temperature characteristic not only by changing the shell thickness but also by changing the outer layer's composition.

Contrary to previous reports [8, 9], phosphorus peak was not detected in the energy-dispersive X-ray fluorescence spectra of the samples (not shown here), demonstrating that most of the ligands were removed from the surfaces of NCs. Therefore, the LTAQ phenomenon in the investigated samples is unrelated to the phase transformation of the organic medium. Based on the temperature-dependent spectral characteristics analyzed above, the nature of the LTAQ phenomenon in the core/shell and core/double shell nanostructures can be understood as follows: At close distances in the solid state, atoms strongly interact with each other, and therefore those in the core/shell interface region of the nanostructure can move out of their equilibrium position in the crystal lattice. This creates defect states that contribute to the reduction in luminescence intensity. Core/shell interface region restructuring at higher temperatures due to the crystal lattice's thermal expansion and the increase in atoms' mobility results in luminescence recovery of the nanostructure. However, further temperature increase on one hand may create defects at the core/shell interface due to the difference in the core and shell materials' thermal expansion coefficients, and on the other hand will activate other luminescence quenching centers, decreasing the emission intensity of the nanostructure.

As pointed out in Figure 8, the linear dependence of the integrated PL intensities on temperature obtained from CdSe/CdS (1 ML) and CdSe/CdS (3 ML) samples in the temperature ranges of 220 - 360 K and 270 - 340 K, respectively, opens up the prospect of creating temperature sensors for biomedical applications.

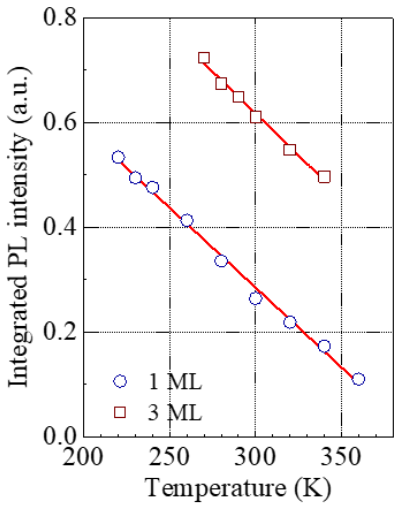

Figure 8. Linear dependencies of integrated emission intensities of CdSe/CdS (1 ML) and CdSe/CdS (3 ML) nanostructures on temperature.

4. CONCLUSIONS

The LTAQ phenomenon was investigated on the CdSe/CdS core/shell and CdSe/CdS/ZnS core/double shell nanostructures. The samples were prepared using the hot injection method. The morphology, XRD and Raman investigations demonstrate the formation of the CdS shell

around the CdSe core. The NC samples have the same core size, CdS shell thicknesses ranging from 1 to 5 ML and ZnS shell thickness of 2 ML. The temperature-dependent PL spectra of these samples were measured in the temperature range of 79 - 460 K with an excitation wavelength of 488 nm. The LTAQ phenomenon was observed in the core/shell and core/double shell nanostructures and is reversible. The luminescence recovery magnitude and the recovery temperature range are different depending on the thickness and composition of the core's surrounding shell. The relation between emission energy and temperature is well described using the Varshni expression. The strong increase in the α thermal coefficient with CdS shell thickness starting from 3 ML shows a significant change of the strain in the core/shell NCs. The cause of the LTAQ phenomenon is attributed to the restructuring of the core/shell and shell/shell interface regions in the investigated nanostructures due to the different thermal expansion coefficients of core and shell materials. The linear variation in the integrated PL intensity in the temperature ranges of 220-360 K and 270 - 340 K for the CdSe/CdS (1 ML) and CdSe/CdS (3 ML) samples, respectively, opens up the prospect of creating temperature sensors for biomedical applications.

Acknowledgements. The present research is funded by International Center of Physics under grant number ICP.2020.09.

CRediT authorship contribution statement. Nguyen Dieu Linh: Conceptualization, Investigation, Data curation, Writing-original draft. Nguyen Thi Thuy Lieu: Methodology, Formal analysis, Funding acquisition. Nguyen Thi Minh Hien: Validation, Writing-review and editing. Nguyen Xuan Nghia: Supervision, Writing-review and editing.

Declaration of competing interest. The authors declare that they have no known competing financial interests or personal relationships that could have appeared to influence the work reported in this paper.

REFERENCES

1. Kim J. C., Rho H., Smith L. M., Jackson H. E., Lee S., Dobrowolska M., and Furdyna J. K. - Temperature-dependent micro-photoluminescence of individual CdSe self-assembled quantum dots, Appl. Phys. Lett. **75** (2) (1999) 214-216. https://doi.org/10.1063/1.124323.
2. Valerini D., Cretí A., Lomascolo M., Manna L., Cingolani R., and Anni M. - Temperature dependence of the photoluminescence properties of colloidal CdSe/ZnS core/shell quantum dots embedded in a polystyrene matrix, Phys. Rev. B, **71** (23) (2005) 235409. https://doi.org/10.1103/PhysRevB.71.235409.
3. Donega C. M., Bode M., and Meijerink A. - Size-and temperature-dependence of exciton lifetimes in CdSe quantum dots, Phys. Rev. B **74** (8) (2006) 805320.

   https://doi.org/10.1103/PhysRevB.74.085320.
4. Zhua C., Longa Zh., Wanga Q., Qiua J., Zhoua J., Zhoua D., Wua H., and Zhu R. - Insights into anti-thermal quenching of photoluminescence from $SrCaGa_4O_8$ based on defect state and application in temperature sensing, J. Lumin. **208** (2019) 284-289. https://doi.org/10.1016/j.jlumin.2018.12.063.
5. Wei Y., Yang H., Gao Z., Yun X., Xing G., Zhou C., and Li G. - Anti-Thermal-Quenching Bi^{3+} Luminescence in a Cyan-Emitting $Ba_2ZnGe_2O_7$:Bi Phosphor Based on Zinc Vacancy, Laser Photonics Rev. **15** (2021) 2000048.

   https://doi.org/10.1002/lpor.202000048.

6. Lei L., Xia J., Cheng Y., Wang Y., Bai G., Xiaa H., and Xu Sh. - Enhancing negative thermal quenching effect via low-valence doping in two-dimensional confined core–shell upconversion nanocrystals, J. Mater. Chem. C **6** (2018) 11587-11592. https://doi.org/10.1039/C8TC04392B.
7. Lei L., Chen D., Li C., Huang F., Zhang J., and Xu Sh. - Inverse thermal quenching effect in lanthanide-doped upconversion nanocrystals for anti-counterfeiting, J. Mater. Chem. C **6** (2018) 5427-5433. https://doi.org/10.1039/C8TC01433G.
8. Wuister S. F., Houselt A. V., Donega C. M., Vanmaekelbergh D., and Meijerink A. - Temperature Antiquenching of the Luminescence from Capped CdSe Quantum Dots, Angew. Chem. Int. Ed. **43** (2004) 3029-3033. https://doi.org/10.1002/ange.200353532.
9. Chin P. T. K., Donega C. M., Bavel S. S., Meskers S. C. J., Sommerdijk N. A. J. M., and Janssen R. A. J. - Highly Luminescent CdTe/CdSe Colloidal Heteronanocrystals with Temperature-Dependent Emission Color, J. Am. Chem. Soc. **129** (48) (2007) 14880-14886. https://doi.org/10.1021/ja0738071.
10. Walker G. W., Sundar V. C., Rudzinski C. M., Wun A. W., Bawendi M. G., and Nocera D. G. - Quantum-dot optical temperature probes, Appl. Phys. Lett., **83** (17) (2003) 3555-3557. https://doi.org/10.1063/1.1620686.
11. Jing P., Zheng J., Ikezawa M., Liu X., Lv Sh., Kong X., Zhao J., and Masumoto Y. - Temperature-Dependent Photoluminescence of CdSe-Core CdS/CdZnS/ZnS-Multishell Quantum Dots, J. Phys. Chem. C **113** (31) (2009) 13545-13550. https://doi.org/10.1021/jp902080p.
12. Ding X., Dai R. C., Zhao Z., Wang Z. P., Sun Z. Q., Zhang Z. M., and Ding Z. J. – Irreversible temperature quenching and antiquenching of photoluminescence of ZnS/CdS:Mn/ZnS quantum well quantum dots, Chem. Phys. Lett. **625** (2015) 147-150. https://doi.org/10.1016/j.cplett.2015.02.049.
13. Agrawal M., Rubio-Retama J., Zafeiropoulos N. E., Gaponik N., Gupta S., Cimrova V., Lesnyak V., Lopez-Cabarcos E., Tzavalas S., Rojas-Reyna R., Eychmuller A., and Stamm M. - Switchable Photoluminescence of CdTe Nanocrystals by Temperature-Responsive Microgels, Langmuir **24** (17) (2008) 9820-9824. https://doi.org/10.1021/la801347d.
14. Battaglia D., Li J. J., Wang Y., and Peng X. - Colloidal Two-Dimensional Systems: CdSe Quantum Shells and Wells, Angew. Chem. Int. Ed. **42** (41) (2003) 5035-5039. https://doi.org/10.1002/anie.200352120.
15. Talapin D. V., Mekis I., Go1tzinger S., Kornowski A., Benson O., and Weller H. - CdSe/CdS/ZnS and CdSe/ZnSe/ZnS Core-Shell-Shell Nanocrystals, J. Phys. Chem. B **108** (49) (2004) 18826-18831. https://doi.org/10.1021/jp046481g.
16. Zhang J., Zhang X., and Zhang J. Y. - Dependence of Microstructure and Luminescence on Shell Layers in Colloidal CdSe/CdS Core/Shell Nanocrystals, J. Phys. Chem. C **114** (9) (2010) 3904-3908. https://doi.org/10.1021/jp9120194.
17. Sharma A.B., Sharma S. K., Sharma M., Pandey R. K., and Reddy D.S. - Structural and optical investigation of semiconductor CdSe/CdS core–shell quantum dot thin films, Spectrochimica Acta Part A **72** (2) (2009) 285-290.

    https://doi.org/10.1016/j.saa.2008.09.031.

18. Lu L., Xu X. L., Liang W. T., and Lu H. F. - Raman analysis of CdSe/CdS core–shell quantum dots with different CdS shell thickness, J. Phys.: Condens. Matter **19** (40) (2007) 406221. https://doi.org/10.1088/0953-8984/19/40/406221.
19. Dzhagan V. M., Valakh M. Y., Raevskaya A. E., Stroyuk A. L., Kuchmiy S. Y., and Zahn D. R. T. - Resonant Raman scattering study of CdSe nanocrystals passivated with CdS and ZnS, Nanotechnology **18** (28) (2007) 285701. https://doi.org/10.1088/09574484/18/28/285701.
20. Tschirner N., Lange H., Schliwa A., Biermann A., Thomsen C., Lambert K., Gomes R., and Hens Z. - Interfacial Alloying in CdSe/CdS Heteronanocrystals: A Raman Spectroscopy Analysis, Chem. Mater. **24** (2) (2012) 311-318.

    https://doi.org/10.1021/cm202947n.
21. Silva A. C. A., Neto E. S. F., da Silva S. W., Morais P. C., and Dantas N. O. - Modified Phonon Confinement Model and Its Application to CdSe/CdS Core-Shell Magic-Sized Quantum Dots Synthesized in Aqueous Solution by a New Route, J. Phys. Chem. C **117** (4) (2013) 1904-1914. https://doi.org/10.1021/jp308500r.
22. Todescato F., Minotto A., Signorini R., Jasieniak J. J., and Bozio R. - Investigation into the Heterostructure Interface of CdSe-Based Core-Shell Quantum Dots Using Surface-Enhanced Raman Spectroscopy, ACS Nano **7** (8) (2013) 6649-6657. https://doi.org/10.1021/nn402022z.
23. Dabbousi B. O., Rodriguez-Viejo J., Mikulec F. V., Heine J. R., Mattoussi H., Ober R., Jensen K. F., and Bawendi M. G. - (CdSe)ZnS Core-Shell Quantum Dots: Synthesis and Characterization of a Size Series of Highly Luminescent Nanocrystallites, J. Phys. Chem. B **101** (46) (1997) 9463-9475. https://doi.org/10.1021/jp971091y.
24. García-Santamaría F., Chen Y., Vela J., Schaller R. D., Hollingsworth J. A., and Klimov V. I. - Suppressed Auger Recombination in "Giant" Nanocrystals Boosts Optical Gain Performance, Nano Lett. **9** (10) (2009) 3482-3488. https://doi.org/10.1021/nl901681d.
25. Liu S. M., Guo H. Q., Zhang Z. H, Li R., Chen W., and Wang Z. G. - Characterization of CdSe and CdSe/CdS core/shell nanoclusters synthesized in aqueous solution, Physica E **8** (2) (2000) 174-178. https://doi.org/10.1016/S1386-9477(99)00260-X.
26. Chen X., Lou Y., Samia A. C., and Burda C. - Coherency Strain Effects on the Optical Response of Core/Shell Heteronanostructures, Nano Lett. **3** (6) (2003) 799-803. https://doi.org/10.1021/nl034243b.
27. Cao L., Huang S., Lu S., and Lin J. - Effect of layer thickness on the luminescence properties of ZnS/CdS/ZnS quantum dot quantum well, J. Colloid Interf. Sci. **284** (2) (2005) 516-520. https://doi.org/10.1016/j.jcis.2004.10.066.
28. Xie R., Kolb U., Li J., Basche T., and Mews A. - Synthesis and Characterization of Highly Luminescent CdSe-Core CdS/$Zn_{0.5}Cd_{0.5}$S/ZnS Multishell Nanocrystals, J. Am. Chem. Soc. **127** (20) (2005) 7480-7488. https://doi.org/10.1021/ja042939g.
29. Varshni Y. - Temperature dependence of the energy gap in semiconductors, Physica **34** (1) (1967) 149-154. https://doi.org/10.1016/0031-8914(67)90062-6.
30. Neeleshwar S., Chen C. L., Tsai C. B, Chen Y. Y., Chen C. C., Shyu S. G., and Seehra M. S. - Size-dependent properties of CdSe quantum dots, Phys. Rev. B **71** (20) (2005) 201307. https://doi.org/10.1103/PhysRevB.71.201307.